



Do instabilities in high-multiplicity systems explain the existence of close-in white dwarf planets?

R. F. Maldonado,¹★ E. Villaver,^{2,3} A. J. Mustill⁴, M. Chávez¹ and E. Bertone¹

¹*Instituto Nacional de Astrofísica, Óptica y Electrónica, Luis Enrique Erro 1, Tonantzintla 72849, Puebla, México*

²*Departamento de Física Teórica, Universidad Autónoma de Madrid, E-28049 Madrid, Spain*

³*Centro de Astrobiología (CAB, CSIC-INTA), ESAC Campus Camino Bajo del Castillo, s/n, Villanueva de la Cañada, E-28692 Madrid, Spain*

⁴*Lund Observatory, Box 43, SE-22100 Lund, Sweden*

Accepted 2020 November 28. Received 2020 November 19; in original form 2020 October 21

ABSTRACT

We investigate the origin of close-in planets and related phenomena orbiting white dwarfs (WDs), which are thought to originate from orbits more distant from the star. We use the planetary architectures of the 75 multiple-planet systems (four, five, and six planets) detected orbiting main-sequence stars to build 750 dynamically analogous templates that we evolve to the WD phase. Our exploration of parameter space, although not exhaustive, is guided and restricted by observations and we find that the higher the multiplicity of the planetary system, the more likely it is to have a dynamical instability (losing planets, orbit crossing, and scattering), that eventually will send a planet (or small object) through a close periastron passage. Indeed, the fraction of unstable four- to six-planet simulations is comparable to the 25–50 per cent fraction of WDs having atmospheric pollution. Additionally, the onset of instability in the four- to six-planet configurations peaks in the first Gyr of the WD cooling time, decreasing thereafter. Planetary multiplicity is a natural condition to explain the presence of close-in planets to WDs, without having to invoke the specific architectures of the system or their migration through the von Zeipel–Lidov–Kozai effects from binary companions or their survival through the common envelope phase.

Key words: Kuiper Belt: general – planets and satellites: dynamical evolution and stability – stars: AGB and post-AGB – circumstellar matter – planetary systems – white dwarfs.

1 INTRODUCTION

Planets commonly found orbiting main-sequence (MS) stars are in jeopardy as their host stars evolve off the MS to the red giant and asymptotic giant branch (AGB) phases (Villaver & Livio 2007). Planet engulfment during the giant phases of the star is guaranteed to occur to certain orbital distances set by a combination of tidal interaction and stellar mass-loss (Villaver & Livio 2009; Kunitomo et al. 2011; Mustill & Villaver 2012; Nordhaus & Spiegel 2013; Villaver et al. 2014). This has a strong dependency on the stellar mass and is quite sensitive to the planetary mass (e.g. Villaver et al. 2014). Several lines of evidence show, however, that both planets and rocky bodies must be dynamically delivered to the white dwarf’s (WD) proximity after the end of the AGB. The first direct transit detection of a Jovian-sized planet candidate in a compact 1.4-d orbit has just been found (Vanderburg et al. 2020), and related observed phenomena such as atmospheric pollution (e.g. Zuckerman et al. 2003), near-infrared excesses (e.g. Gänsicke et al. 2006), asteroids (Vanderburg et al. 2015; Manser et al. 2019; Vanderbosch et al. 2020), or even planets inferred from a gas disc (Gänsicke et al. 2019) have been reported for years.

As a star becomes a WD, it loses a considerable fraction of its mass; this moves the planets on to wider orbits, but also leads to an increase

of the planet:star mass ratio, which radically changes the dynamics and stability of multiple planetary systems. The pioneering work of Debes & Sigurdsson (2002) that explored the effects of mass-loss on dynamical evolution has been followed by many studies of two-planet systems (Veras & Mustill 2013; Veras et al. 2013; Voyatzis et al. 2013; Smallwood et al. 2018; Maldonado et al. 2020a; Ronco et al. 2020). However, similar studies using three and four planets in generic planetary systems are more scarce (Mustill, Veras & Villaver 2014; Veras & Gänsicke 2015; Veras et al. 2016; Mustill et al. 2018; Maldonado et al. 2020b). The overall conclusion of all these works is that instabilities that lead to the loss of a planet in two- and three-planet systems do not occur often enough to explain the high incidence of atmospheric pollution observed in WDs, even when considering instabilities such as orbit crossing and orbital scattering.

The point we make in the present letter is that a high multiplicity of planets increases the planet–planet scattering events that lead to dynamical instabilities that eventually pollute WDs and drive planets and/or asteroids to its close vicinity. Furthermore, we provide a natural mechanism to explain the presence of planets reaching close orbits around WDs, without having to invoke the specific architecture of the system as a hierarchical quadruple to explain its migration through the von Zeipel–Lidov–Kozai effect (von Zeipel 1910; Kozai 1962; Lidov 1962), as has been done for the recently discovered WD 1856 b (Vanderburg et al. 2020) in O’Connor, Liu & Lai (2020), Muñoz & Petrovich (2020), and Stephan, Naoz & Gaudi (2020). For the first time, we study the post-MS dynamical

* E-mail: raulfms@inaoep.mx

evolution of four- to six-planet systems by using scaled versions of the planetary architectures observed orbiting MS stars. We also expand the previously explored parameter space.

2 NUMERICAL SIMULATIONS SET-UP

In Maldonado et al. (2020a, b, Papers I and II from now onwards), we evolved the planetary architectures of the two- and three-planet systems. Here, we follow the same procedure to simulate the evolution of higher multiplicity (four, five, and six) detected planetary systems orbiting MS stars. To do so, first, we obtain from the Exoplanet Encyclopedia (Schneider et al. 2011),¹ and the NASA Exoplanet Archive (Akeson et al. 2013)² 51 four-planet systems, 14 five-planet systems, and 10 six-planet systems with reported discovery up to September 2020, excluding from this list close binaries and pre-MS stars. The final sample used in this work contains a total of 75 MS stars. From the observations, we select the planet and stellar masses, radius, and eccentricity, when available. If not available, as in Papers I and II, we have used a standard planet mass–radius relation (Chen & Kipping 2017), and Rayleigh distributions with a σ parameter $\sigma = 0.02$ (Pu & Wu 2015) for the eccentricity, and with $\sigma = 1.12^\circ$ (Xie et al. 2016) for the inclination angles. For each observed template system, we run 10 clones, differing in the randomisation of their orbital phases and orientations.

The host stars that originally span a mass range from 0.27 to $1.56 M_\odot$ have been re-scaled to a $3 M_\odot$ mass star, while keeping them dynamically analogous to the original system. A $3 M_\odot$ star represents the average MS mass of observed polluted WDs ($\sim 0.7 M_\odot$; Koester, Gänsicke & Farihi 2014) and allows us to follow the evolution to the WD in a feasible computational time. If lower mass progenitors were considered, we would expect slightly fewer systems to become unstable, as they lose a slightly smaller fraction of their mass in becoming a WD (Mustill et al. 2014). The evolution of the star has been computed using the SSE code (Hurley, Pols & Tout 2000) assuming the Reimers mass-loss parameter $\eta = 0.5$ and solar metallicity. The planetary masses have been re-scaled as well, to conserve the dynamical properties (multiplying the planet mass by the ratio between the modelled and the observed stellar mass in the system).

We use the MERCURY package (Chambers 1999) modified by (Veras et al. 2013; Mustill et al. 2018) with an implemented RADAU integrator with a tolerance parameter of 10^{-11} as in Mustill et al. (2018) and Papers I and II to evolve the planetary systems from the start of the MS for 10 Gyr. Planets are removed from the simulations when they reach an orbital distance of 1×10^6 au from the central star, which we consider an ejection. Planets colliding with each other or with the stellar radius are also removed. To avoid the complications of tidal evolution on the AGB and ensure their survival to engulfment, we placed the innermost planet (planet 1) at a semimajor axis $a_0 = 10$ au (see Villaver & Livio 2009; Mustill & Villaver 2012). We assure the conservation of the dynamics of the system by placing consecutive pairs at distances $(a_j/a_1)a_0$ (where a_1 , and a_j are the observed semimajor axes of planets 1 and j (with $2 \leq j \leq 6$), respectively).

In Fig. A1 (see appendix), we present histograms of the planet mass distribution (left-hand panel) and the eccentricity distribution (middle panel) of the simulated planets using different colours according to the number of planets in the system. We have added

in (light) black, for reference, the distribution of the two- and three-planet systems simulated in Papers I and II. The right-hand panel of Fig. A1 displays the distribution of Δ (in mutual Hill units defined as $\Delta = (a_j - a_i)/R_{m, \text{Hill}}$, where i, j indicates a planet pair i – j and $R_{m, \text{Hill}}$ is the mutual Hill radius of the planet pair) for adjacent pairs of planets.

3 RESULTS

We have performed a total of 750 simulations (10 simulations per system configuration) where 510, 140, and 100 are of four-, five-, and six-planet systems, respectively. We have removed from the following analysis all the planetary systems that have at least one pair of planets in mean motion commensurabilities, which produce planet losses and orbit crossing on the MS. That is the case for a total of 167 simulations (105 are in 12 systems with four planets, 12 in 3 systems with five planets, and 50 in 6 systems of six planets).

In Table 1, we present the numbers and percentages of planets lost by different dynamical instabilities on the WD phase. We count only different simulations where at least one planet is lost. In Fig. 1, we display the fraction of systems losing planets either by Hill (planets collide with each other or their orbits cross) or Lagrange instabilities (ejected or collide with the star) with respect to the number of simulations in each planetary configuration (including those from Papers I and II). We see that as the multiplicity of planets increase, the fraction of instabilities also increases.

It is important to note that planet ejections not only happen more frequently in our four- to six-planet simulations, but also that the surviving planets remain dynamically active after the ejection, having eccentricity excitation that produces several orbit crossings. A planetesimal belt, if present, could be disrupted that way. We have a non-negligible number of simulations where, despite no planets being lost, there is orbit crossing and orbital scattering during the WD phase. We have listed those in Table 1 and added them to the total contribution to the WD pollution in the last line of the table. Indeed Mustill et al. (2018) show that planets having a mass $\leq 100 M_\oplus$ (low-mass planets) are efficient deliverers of planetesimals toward the WD. The percentage of our simulations with low-mass planets involved in simulations dynamically active is high ~ 65 per cent for planet masses in the range of 0.9 – $85 M_\oplus$ in the four- and five-planet system simulations and low ~ 10 per cent in the six-planet system case.

Planets can be sent to very close distances (even crossing the Roche radius) of the WD. As an example of a system with a complex dynamical behaviour, we show in Fig. 2 the scaled system *Kepler*-84: several orbit crossings occur among the five planets, producing the ejections of planets 4 and 5, while planets 2 and 5 have such a high eccentricity excitation that cause both planets to have several pericentre passages within the WD Roche radius. The number of simulations that have at least one planet having pericentre passages up to 10 Roche radii of the WD is listed in Table 1 as well as the number of them that indeed cross the Roche radius. Some simulations have more than one planet crossing the Roche radius. Reported in the planet–star collision row of Table 1 are the planets that entered the Roche radius and finally collided with the WD.

The times at which the instability events happen are shown in Fig. 3. The left-hand panel is the cooling time of the first orbit crossing with and without planet losses, and the right-hand one reflects when the planet losses happen. We have a peak in the number of orbit crossing and planet losses in the first Gyr but with the orbit crossing events slowing down as the WD ages (only a slight increase around 7 Gyr in the four-planet case) and the planet losses maintained

¹<http://exoplanet.eu/>

²<https://exoplanetarchive.ipac.caltech.edu/>

Table 1. Instabilities at the WD phase according to the number of planets in the simulated system. The first percentage is given with respect to the total number of simulations and the second one is the fraction with respect to the total number of planets. Note that several planets are lost in the same simulation and some with different instability type; however, the total number of systems reflects only different simulations where a planet is lost.

	Two-planet systems		Three-planet systems		Four-planet systems		Five-planet systems		Six-planet systems	
	Systems	Planets	Systems	Planets	Systems	Planets	Systems	Planets	Systems	Planets
Ejections	68 (2.0 %)	68 (1.0 %)	69 (5.9 %)	71 (2.0 %)	46 (11.4 %)	67 (4.1 %)	41 (32.0 %)	74 (11.6 %)	24 (48.0 %)	57 (19.0 %)
Planet–star collisions	5 (0.1 %)	5 (0.1 %)	9 (0.8 %)	9 (0.3 %)	11 (2.7 %)	11 (0.7 %)	15 (11.7 %)	15 (2.3 %)	5 (10.0 %)	5 (1.7 %)
Planet–planet collisions	7 (0.2 %)	7 (0.1 %)	–	–	1 (0.3 %)	1 (0.1 %)	–	–	2 (4.0 %)	2 (0.7 %)
Planets within 10 Roche radii	8 (0.2 %)	8 (0.1 %)	26 (2.2 %)	30 (0.9 %)	29 (7.2 %)	47 (2.9 %)	32 (25.0 %)	48 (7.5 %)	14 (28.0 %)	23 (7.7 %)
Planets within 1.4-d orbits	8 (0.2 %)	8 (0.1 %)	22 (1.9 %)	26 (0.8 %)	27 (6.7 %)	40 (2.5 %)	32 (25.0 %)	47 (7.3 %)	12 (24.0 %)	18 (6.0 %)
Planets entering the Roche radius	7 (0.2 %)	7 (0.1 %)	19 (1.6 %)	22 (0.6 %)	23 (5.7 %)	33 (2.0 %)	30 (23.4 %)	45 (7.0 %)	12 (24.0 %)	16 (5.3 %)
Orbit crossing and planet losses	26 (0.8 %)	–	63 (5.4 %)	–	52 (12.8 %)	–	45 (35.2 %)	–	26 (52.0 %)	–
Orbit crossing and/or scattering without planet losses	32 (0.9 %)	–	24 (2.1 %)	–	26 (6.4 %)	–	2 (1.6 %)	–	6 (12.0 %)	–
Total (losing planets)	80 (2.3 %)	80 (1.2 %)	76 (6.6 %)	80 (2.3 %)	52 (12.8 %)	79 (4.9 %)	45 (35.2 %)	89 (13.9 %)	26 (52.0 %)	64 (21.3 %)
Total (WD pollution)	112 (3.2 %)	–	100 (8.6 %)	–	78 (19.3 %)	–	47 (36.7 %)	–	32 (64.0 %)	–
Total (for statistics)	3485	6970	1160	3480	405	1620	128	640	50	300

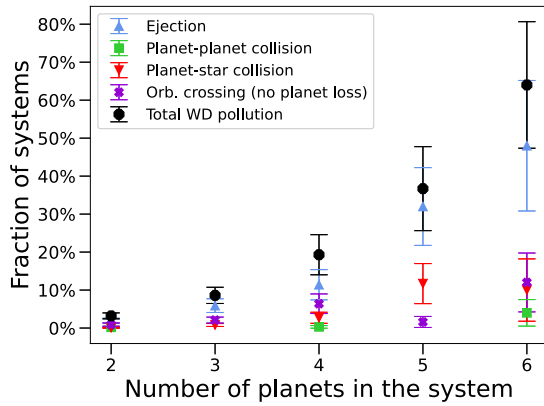


Figure 1. Relative number of multiple-planet systems with respect to the total number of simulations losing planets by Hill and/or Lagrange instabilities as well as the simulations with orbit crossing that do not lose any planet during 10 Gyr. Additionally, we present the total number of simulations that may contribute to WD pollution. Error bars correspond to the standard deviation of the Bootstrap resampling method. Each instability type is marked with a different symbol and colour.

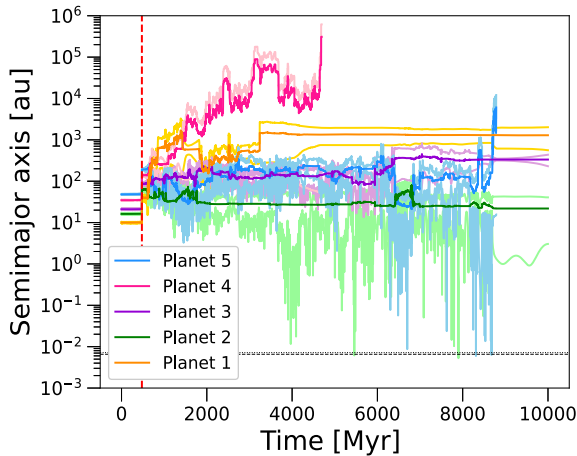


Figure 2. Semimajor axis evolution of the scaled five-planet system *Kepler-84*. Planets are displayed with different colours, with the lighter version of the colours showing the pericentre and apocentre. The red vertical dashed line indicates the beginning of the WD phase. The black dotted and dashed lines show the WD Roche radius for planet 2 (mass $21.7 M_{\oplus}$) and 5 (mass $68.6 M_{\oplus}$), respectively.

at lower rates throughout the simulated times. Most of the planet losses are ejections but, as mentioned before, the surviving planets continue being dynamically active. In the upper part of the right-hand panel, we show the cooling time when planet–star collisions happen. We see that this outcome spans up to 8 Gyr of cooling time (four- and five-planet systems) and only systems with six planets have collisions restricted to 4 Gyr. The time of the destabilizing events has a dependency on the mass of the planets involved. Multi-planet systems having at least one planet with $M > 100 M_{\oplus}$ tend to destabilize earlier than their low-mass counterparts. As an example, in the four-planet case, orbit crossing events have a median time of 53.9 Myr and 1.08 Gyr in the high-mass and low-mass cases, respectively (same numbers for the planet losses are 454.5 Myr and 1.54 Gyr, respectively).

4 DISCUSSION

Previous studies on the post-MS evolution of planetary systems of high multiplicity are very limited and mostly restricted to four-planet systems. For instance, Veras & Gänsicke (2015) and Veras et al. (2016) obtained a much larger fraction of unstable (here, unstable includes losing planets and/or having orbit crossing on the WD phase and excludes the MS unstable systems) four-planet system simulations (44.7 per cent and 73.0 per cent, respectively) than this work (19.3 per cent). Furthermore, all the 19 simulations of six- and eight-planets in Veras et al. (2016) and the 40 simulations that Veras & Gänsicke (2015) performed using 10 Earth-mass planets become unstable in the WD phase. The main reason behind the different percentages obtained is easily appreciated in the right-hand panel of Fig. A1. Previous works have probed packed systems (maximum 15 in mutual Hill radii for terrestrial planets and 8 for Jovian planets) whereas we have used adjacent planet pairs with Δ values up to 66.3 mutual Hill radii. Note that only 36 per cent of our tested four-planet pairs are in the range between 4 and 15 mutual Hill radii tested previously and 12 per cent have planets in adjacent pairs with Δ between 6 and 10 in the six-planet systems.

The majority of planets in the WD phase are lost due to ejections in our simulations (see Table 1) and that is what has been found as well in previous works where planet ejections are the most prominent instability outcome (Veras & Mustill 2013; Veras et al. 2013, 2016; Mustill et al. 2014; Mustill et al. 2018; Maldonado et al. 2020a, b). The percentage of unstable simulations (where planets are lost or are kept the entire simulated time but do experience orbit crossing and/or

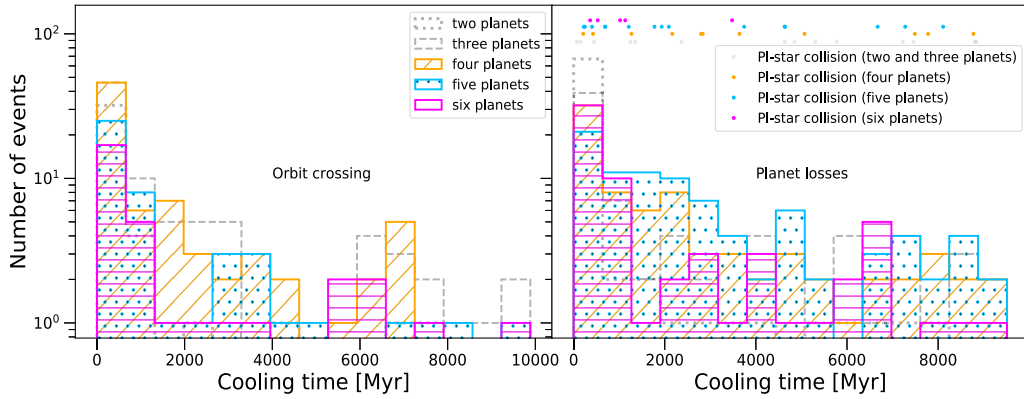


Figure 3. Left-hand panel: Distribution of cooling time of the first orbit crossing. Right-hand panel: The same as the left-hand panel but showing the cooling time when planets are lost by Hill or Lagrange instabilities. The dots in the upper part indicate the time when planet–star collisions happen and different colours refer to systems with different numbers of planets.

orbital scattering) increases with the multiplicity of the planetary system. We cannot attribute this result to having simulated more packed systems (see Fig. A1) nor to small number statistics. We see a significant trend in systems experiencing instability with multiplicity (see Fig. 1)³. Our results show that a higher multiplicity of planets may seem to increase the chance of WD pollution, as the destabilized planets can destabilize asteroid belts, sending the asteroids towards the WD and polluting its atmosphere.

Recently, the first transiting planet has been discovered in a very tight orbit around a WD (Vanderburg et al. 2020): a candidate orbiting the star WD 1856+534 with a mass $\leq 11.7 M_J$ and with a period of 1.4 d. The evolution of the star prevents this planet from being there in such a close orbit (see e.g. Villaver & Livio 2007; Mustill & Villaver 2012; Villaver et al. 2014), unless it survives a common envelope phase (Lagos et al. 2020). Thus, dynamical instabilities among outer bodies must be invoked to explain its presence.

We find in our simulations several planets that approach the surroundings of the WD following dynamical instabilities (note the closest planet is always located at 10 au at the start of the simulations). The number of planets reaching pericentre distances ≤ 10 Roche radii (listed in Table 1) is large: 46 planets (with a mass range of 3.3–35.2 M_\oplus) and one planet with a mass of 460.8 M_\oplus in the four-planet systems; 48 planets with masses between 1.5 and 68.6 M_\oplus in the five-planet systems, and 23 planets covering a mass range of 6.2–106 M_\oplus in the six-planet systems simulations.

Only one massive planet $M > 1 M_J$ crosses the 10 Roche radii threshold despite constituting 6.4 per cent of the simulated planets. If we restrict the masses to $\geq 0.1 M_J$ that represent 33.9 per cent of the total planets simulated, we find 24 planets (0.9 per cent of the sample) that reach 10 Roche radii. We find that mostly super-Earth to Saturn-like planets reach close WD distances. Finally, 7.2 per cent, 25 per cent, and 28 per cent of simulations have pericentre passages ≤ 10 Roche radii and 5.7 per cent, 23.4 per cent, and 24 per cent do cross the Roche radius in the four-, five-, and six-planet systems, respectively. We have obtained a higher but comparable fraction of

simulations with planets crossing the Roche radius in the four-planet systems with respect to the two- and three-planet case (less than 2 per cent found in Paper I and II). However, the fraction is higher (~ 24 per cent) in the five- and six-planet case.

Our exploration of parameter space, although not exhaustive, is guided and restricted by observations. We find that higher the multiplicity of the planetary system, the more likely it is to have a dynamical instability that eventually will send a planet (or small object) on to an orbit with a small periastron distance. A similar conclusion was reached by Veras & Gänsicke (2015) in a much more limited analysis. We also find that small planets are more likely to be destabilized on to an orbit passing close to the WD and therefore most likely to be present and/or disrupted and destroyed by tidal forces, leading to the formation of debris or gaseous discs that could eventually pollute the WD atmosphere (Manser et al. 2019; Veras & Fuller 2019).

Note that several studies have attempted to predict the number of planetary systems harbouring multiple planets since observations are biased. Zink, Christiansen & Hansen (2019) provide corrections to the incomplete transit multiplicity of the *Kepler* data and estimate that the average number of planets per G, K dwarf within the radius and period parameter space of *Kepler* to be 5.86 ± 0.18 . Also 32.3 ± 2.7 per cent of solar-like stars should contain at least eight planets within 500 d.

5 CONCLUSIONS

We have performed 750 dynamical simulations of 75 detected MS planetary systems with four, five, and six planets (10 simulations per system configuration). We find that when increasing the multiplicity of the planetary systems studied, the planet–planet scattering events (losing planets, orbit crossing, and scattering) that may contribute to WD pollution (enhanced if putative asteroid belts are present within the system) increase as well. Indeed, the fraction of four- to six-planet unstable simulations is comparable to the 25–50 per cent fraction of WDs having atmospheric pollution (Zuckerman et al. 2003; Koester et al. 2014; Wilson et al. 2019). Additionally, the orbit crossing and planet losses in the four-to-six planetary configurations peak in the first Gyr of the WD cooling time, decreasing as the WD ages.

Our multiple-planet simulations resulted in a non-negligible fraction of planets reaching orbits within the 10 Roche radii of the WD (some of them crossing the Roche radius and even colliding with the WD), especially in systems with five and six planets with planet

³We determine the errors on the instability fractions by means of bootstrap resampling. Because different simulations based on the same template system cannot be regarded as completely independent, we perform a ‘two-layer’ bootstrap, first drawing with replacement from the template systems, and then drawing with replacement from the simulation results for each resampled system. This leads to somewhat larger errors than are obtained by pooling all the simulation results and treating them independently.

masses in the range between super-Earth and Saturn. This confirms that planet–planet scattering in multiple-planet systems leads to the existence of close-in planets around the WD, possibly explaining the origin of the newly discovered WD 1856 b orbiting in a 1.4-d period (Vanderburg et al. 2020). Furthermore, these planets or asteroids can be influenced by tidal forces of the WD (Veras & Fuller 2019; Veras et al. 2019) forming debris discs (Gänsicke et al. 2006; Kilic & Redfield 2007; Farihi 2016; Wilson et al. 2019), with some of them having gaseous components (Melis et al. 2012; Manser et al. 2016, 2020; Melis et al. 2020); producing photoevaporation of their atmospheres (Gänsicke et al. 2019) or having the rocky bodies themselves (Vanderburg et al. 2015; Manser et al. 2019; Vanderbosch et al. 2020) producing WD atmospheric pollution.

ACKNOWLEDGEMENTS

This research has made use of the NASA Exoplanet Archive, which is operated by the California Institute of Technology, under contract with the National Aeronautics and Space Administration under the Exoplanet Exploration Program. This research has made use of the SIMBAD database, operated at CDS, Strasbourg, France. EV and RFM acknowledge support from the ‘On the rocks II project’ funded by the Spanish Ministerio de Ciencia, Innovación y Universidades under grant PGC2018-101950-B-I00 and the Unidad de Excelencia ‘María de Maeztu’ – Centro de Astrobiología (CSIC/INTA). MC, RFM, and EB thank CONACYT for financial support through grant CB-2015-256961. AJM acknowledges support from the starting grant 2017-04945 ‘A unified picture of white dwarf planetary systems’ from the Swedish Research Council. We are grateful to Francisco Prada for the use of the computer cluster to Paul McMillan for statistical advice and to the referee for giving helpful comments to improve the manuscript.

DATA AVAILABILITY

The data underlying this article will be shared on reasonable request to the corresponding author.

REFERENCES

Akeson R. L. et al., 2013, *PASP*, 125, 989
 Chambers J. E., 1999, *MNRAS*, 304, 793
 Chen J., Kipping D., 2017, *ApJ*, 834, 17
 Debes J. H., Sigurdsson S., 2002, *ApJ*, 572, 556
 Farihi J., 2016, *New Astron. Rev.*, 71, 9
 Gänsicke B. T., Marsh T. R., Southworth J., Rebassa-Mansergas A., 2006, *Science*, 314, 1908
 Gänsicke B. T., Schreiber M. R., Toloza O., Fusillo N. P. G., Koester D., Manser C. J., 2019, *Nature*, 576, 61
 Hurley J. R., Pols O. R., Tout C. A., 2000, *MNRAS*, 315, 543
 Kilic M., Redfield S., 2007, *ApJ*, 660, 641
 Koester D., Gänsicke B. T., Farihi J., 2014, *A&A*, 566, A34

Kozai Y., 1962, *AJ*, 67, 591
 Kunitomo M., Ikoma M., Sato B., Katsuta Y., Ida S., 2011, *ApJ*, 737, 66
 Lagos F., Schreiber M. R., Zorotovic M., Gänsicke B. T., Ronco M. P., Hamers A. S., 2020, *MNRAS*, preprint (arXiv:2010.09747)
 Lidov M. L., 1962, *Planet. Space Sci.*, 9, 719
 Maldonado R. F., Villaver E., Mustill A. J., Chavez M., Bertone E., 2020a, *MNRAS*, 497, 4091
 Maldonado R. F., Villaver E., Mustill A. J., Chavez M., Bertone E., 2020b, *MNRAS*, 499, 1854
 Manser C. J., Gänsicke B. T., Koester D., Marsh T. R., Southworth J., 2016, *MNRAS*, 462, 1461
 Manser C. J. et al., 2019, *Science*, 364, 66
 Manser C. J., Gänsicke B. T., Gentile Fusillo N. P., Ashley R., Breedt E., Hollands M., Izquierdo P., Pelisoli I., 2020, *MNRAS*, 493, 2127
 Melis C. et al., 2012, *ApJ*, 751, L4
 Melis C., Klein B., Doyle A. E., Weinberger A. J., Zuckerman B., Dufour P., 2020, preprint (arXiv:2010.03695)
 Muñoz D. J., Petrovich C., 2020, *ApJ*, 904, L3
 Mustill A. J., Villaver E., 2012, *ApJ*, 761, 121
 Mustill A. J., Veras D., Villaver E., 2014, *MNRAS*, 437, 1404
 Mustill A. J., Villaver E., Veras D., Gänsicke B. T., Bonsor A., 2018, *MNRAS*, 476, 3939
 Nordhaus J., Spiegel D. S., 2013, *MNRAS*, 432, 500
 O’Connor C. E., Liu B., Lai D., 2020, *MNRAS*, preprint (arXiv:2010.04163)
 Pu B., Wu Y., 2015, *ApJ*, 807, 44
 Ronco M. P., Schreiber M. R., Giuppone C. A., Veras D., Cuadra J., Guilera O. M., 2020, *ApJ*, 898, L23
 Schneider J., Dedieu C., Le Sidaner P., Savalle R., Zolotukhin I., 2011, *A&A*, 532, A79
 Smallwood J. L., Martin R. G., Livio M., Lubow S. H., 2018, *MNRAS*, 480, 57
 Stephan A. P., Naoz S., Gaudi B. S., 2020, preprint (arXiv:2010.10534)
 Vanderbosch Z. et al., 2020, *ApJ*, 897, 171
 Vanderburg A. et al., 2015, *Nature*, 526, 546
 Vanderburg A. et al., 2020, *Nature*, 585, 363
 Veras D., Fuller J., 2019, *MNRAS*, 489, 2941
 Veras D., Gänsicke B. T., 2015, *MNRAS*, 447, 1049
 Veras D., Mustill A. J., 2013, *MNRAS*, 434, L11
 Veras D., Mustill A. J., Bonsor A., Wyatt M. C., 2013, *MNRAS*, 431, 1686
 Veras D., Mustill A. J., Gänsicke B. T., Redfield S., Georgakarakos N., Bowler A. B., Lloyd M. J. S., 2016, *MNRAS*, 458, 3942
 Veras D. et al., 2019, *MNRAS*, 486, 3831
 Villaver E., Livio M., 2007, *ApJ*, 661, 1192
 Villaver E., Livio M., 2009, *ApJ*, 705, L81
 Villaver E., Livio M., Mustill A. J., Siess L., 2014, *ApJ*, 794, 3
 von Zeipel H., 1910, *Astron. Nachr.*, 183, 345
 Voyatzis G., Hadjidemetriou J. D., Veras D., Varvoglis H., 2013, *MNRAS*, 430, 3383
 Wilson T. G., Farihi J., Gänsicke B. T., Swan A., 2019, *MNRAS*, 487, 133
 Xie J.-W. et al., 2016, *Proc. Natl. Acad. Sci.*, 113, 11431
 Zink J. K., Christiansen J. L., Hansen B. M. S., 2019, *MNRAS*, 483, 4479
 Zuckerman B., Koester D., Reid I. N., Hünsch M., 2003, *ApJ*, 596, 477

APPENDIX A: ADDITIONAL MATERIAL

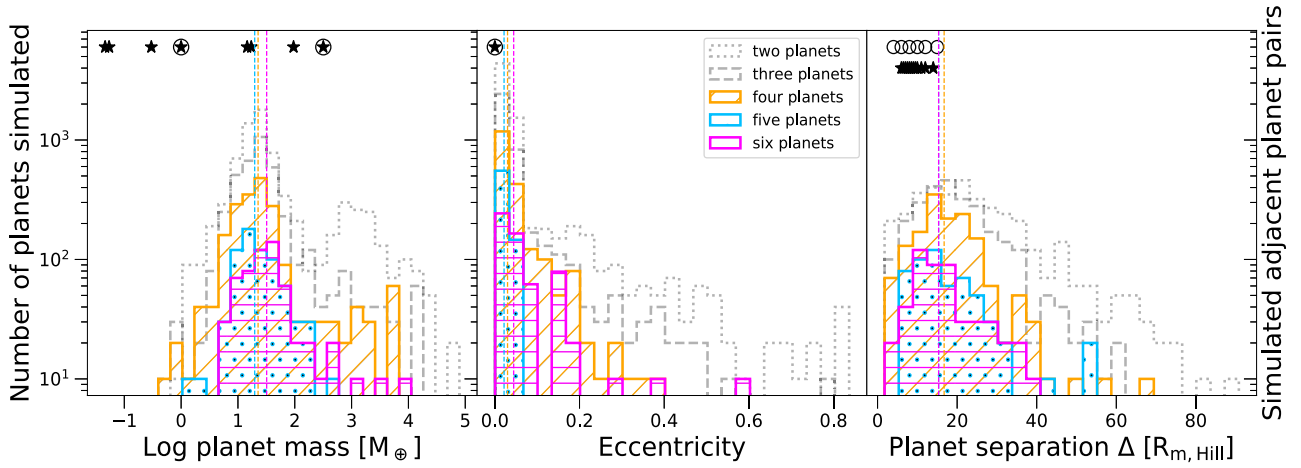


Figure A1. Left-hand panel: Histograms of the simulated planet masses, different colours are for the planetary system according to the number of planets (see legend). Middle panel: Same as the left-hand panel but for the planet eccentricities. Right-hand panel: Planet separation Δ in mutual Hill units of adjacent pairs of planets. Symbols in the upper part are the values used in previous works: black star and circles for Veras et al. (2016) and Veras & Gänsicke (2015), respectively. The medians of the planet mass (plotted as dashed vertical lines) are 22.6, 19.7, and 32.0 M_{\oplus} for the four-, five-, and six-planet systems, respectively. For the eccentricity: four-planet, five-planet, and six-planet systems have a median of 0.03, 0.02, and 0.05, respectively. The medians of the planet separation Δ of the adjacent planet pairs are 16.7, 15.4, and 15.3 for the four-, five-, and six-planet systems, respectively.

This paper has been typeset from a \LaTeX file prepared by the author.